Re-Evaluation of Factors Controlling Landslides Triggered by the 1999 Chi–Chi Earthquake

22

Chyi-Tyi Lee

Abstract

Landslides triggered by the 1999 Chi–Chi earthquake were re-mapped from high-resolution SPOT images taken before and after the quake. Their distribution was studied and landslide controlling factors statistically analyzed. Slope gradient, relative slope height, total slope height, closest distance to fault-rupture plane, and Arias Intensity were the most significant factors affecting landsliding. Earthquake-induced landslides were most common on longer and steeper slopes, and occurred at a high position on the slope. Most landslides were concentrated in the regions with peak ground accelerations exceeding 250 gals.

Keywords

Landslide · Earthquake-induced landslide · Controlling factor · Topographic amplification

1 Introduction

At 1:47 a.m. local time on September 21, 1999, a shallow M_W7.6 earthquake struck central Taiwan rupturing the Chelungpu fault. The hypocenter was 8 km below the village of Chi–Chi. The main shock severely shook the entire island of Taiwan (Ma et al. 1999; Kao and Chen 2000) causing considerable structural damage and triggering thousands of landslides.

Rapid mapping of landslides from SPOT images for the whole of Taiwan was carried out by Liao and Lee (2000). They documented 9,272 larger landslides of various types (with areas >625 m^2) with a total area of 127.8 km^2. Wang et al. (2002), based on interpretation from aerial photos of the meizoseismal area in central Taiwan, recognized more than twenty-thousand landslides. Factors controlling the earthquake-induced landslides were evaluated by Khazai and Sitar (2003) based on a preliminary landslide inventory. The satellite images used in my work in 2,000 were not at a high resolution and were analyzed in a hurry, so we re-mapped the earthquake-induced landslides from high-resolution SPOT images, and checked using aerial photo-pairs from 2003 to 2008. Landslide types were

C.-T. Lee (✉)
Graduate Institute of Applied Geology, National Central University, Taiwan, No. 300, Jhongda Rd, Jhongli City, Taoyuan County 32001, Taiwan
e-mail: ct@ncu.edu.tw

K. Ugai et al. (eds.), *Earthquake-Induced Landslides*,
DOI: 10.1007/978-3-642-32238-9_22,

recognized, deposit areas were separated, and a GIS database was built.

This paper describes the landslide mapping, presents an overview of landslide distribution, basic statistics of factors associated with the landslides, and interpretation of effective factors controlling the landslides. We also discuss the characteristics of the earthquake-induced landslides, which provide insight into where and why earthquake landslides occur.

2 Regional Setting

The island of Taiwan has an area of 36,000 km^2. The highest peak is Yushan, which is 3,952 m above sea level, and numerous other peaks rise to over 3,000 m. Taiwan is tectonically active, as it is in the collision zone between the Asiatic continent and the Luzon Arc (Teng 1990). Active crustal deformation (Bonilla 1975; Yu et al. 1997), frequent earthquakes (Tsai et al. 1977; Wu 1978), numerous typhoons and a high erosion rate (Dadson et al. 2003) presently affect the region.

The island has a north–south running backbone range, surrounded by foothills and coastal plains. Geologically, the range has a metamorphic core, surrounded by slate formations, and fold-and-thrust Neogene sedimentary strata. The Chelungpu fault, which ruptured during the Chi–Chi earthquake, is a thrust fault in the fold-and-thrust belt. A coastal plain and gentle slopes lie to the west of the fault, and hills and high mountains to the east. The majority of the earthquake-induced landslides were located east of the fault.

The climate in Taiwan area is subtropical, with an average annual precipitation of about 2,500 mm. No significant precipitation was observed within 1 month before and for a half month after the Chi–Chi earthquake, simplifying the study of earthquake-induced landslides.

3 Methodology

In this study, we used SPOT satellite images and aerial photographs to identify the landslides, and MapInfo GIS software to digitize their location and extent. Spatial distribution, as well as numbers and areas of landslides triggered by the Chi–Chi earthquake, were then mapped. Spatial functions in GIS were used to analyze the relationships between the landslide distribution and factors associated with the landslides. Erdas Imagine system was used to process DEM and derive topographic factors for statistics. Strong-motion data were processed using a standardized method by FORTRAN code, and the ground-motion values were interpolated on each grid point in the study area using ordinary Kriging.

3.1 Methods for Evaluating the Effectiveness of a Factor

If a factor can be used to interpret the landslide spatial distribution to some extent, this factor is an effective factor. We propose three different methods to evaluate the effectiveness of a factor. For any given factor, the data set is divided into a *landslide* group and a *non-landslide* group for analysis. Theoretically, if the two groups have almost no intersection and can be easily separated, then this factor should be a perfectly effective factor. If the percentage of landslides increases or decreases with the factor score, then this factor is considered an effective factor.

Flat areas and gentle slopes where the slope gradient is <10 % with an area >1 ha are regarded as stable and were not included in either the *non-landslide* or *landslide* groups. Stable areas were not included in the analysis.

Difference Between *landslide* and *Non-landslide* Groups

The difference between two groups can be visually inspected by plotting the frequency distribution of the two groups and quantified by computing a standardized difference D (Davis 2002) from which the effectiveness of a factor as discriminator can be determined:

$$D_j = \frac{\bar{A}_j - \bar{B}_j}{S_{Pj}}, \tag{22.1}$$

where $\bar{A}_j$ is the mean of factor j for group A (landslide); $\bar{B}_j$ is the mean of factor j for group B (non-landslide); S_{Pj} is the pooled standard deviation of factor j; and D_j is standardized difference of factor j. The larger the standardized difference, the more effective the factor.

Before calculating the standardized difference of a factor, a test of normality is required. A standardized difference value for evaluation is valid only for a normal distributed data set.

Correlation Between Landslide Ratio and the Factor Scores

An effective factor should be correlated with the proportion of landslide cells (Jibson et al. 2000) or the landslide ratio (landslide pixels to total pixels ratio in a factor interval) (Lee et al. 2005). The correlation can be visually inspected by plotting the landslide ratio against the factor score. A correlation coefficient may also be calculated; either a positive or a negative correlation is good for an effective factor.

A threshold may exist for landslides. When the factor score is less than the threshold, the landslide ratio may be zero. Only factor scores greater than the threshold are needed in the calculation of a correlation coefficient. Either probability of failure or landslide probability is used in the following description with the term—landslide ratio.

Success Rate Curve

The success rate curve was firstly proposed by Chung and Fabbri in 1999. It is a cumulative landslide ratio calculated starting from the highest susceptibility of a model. The success rate of a factor is calculated starting from the lowest factor score if there is positive correlation between landslide ratio and factor score; or starting from the highest factor score if there is a negative correlation.

The curve indicates how well a model (or a factor) interprets the data (landslides). The success rate curve has an area under the curve (AUC). This area is between 0 and 1; a higher value indicates a higher success rate, whereas a value near or <0.5 means the factor is not effective at all. In the model evaluation, we used to classify $AUC \geq 0.9$ as excellent, $0.9 > AUC \geq 0.8$ as good, $0.8 > AUC \geq 0.7$ as fair, $0.7 > AUC \geq 0.6$ as poor, $AUC < 0.6$ as very poor (Lee et al. 2008a, b). In the present evaluation of factors, we classify $AUC \geq 0.8$ as excellent, $0.8 > AUC \geq 0.7$ as good, $0.7 > AUC \geq 0.6$ as fair, $0.6 > AUC \geq 0.55$ as poor, and $AUC < 0.55$ as very poor.

4 Data Acquisition and Processing

The basic data used in this study included SPOT images, a 5-m grid digital elevation model (DEM), 1/5,000 photo-based contour maps, 1:50,000 geologic maps, and earthquake strong-motion records. SPOT images taken before and just after the Chi–Chi earthquake were selected for use and are listed in Table 22.1. The SPOT images were received, processed and rectified by the Center for Space and Remote Sensing Research, National Central University, Taiwan. Both multi-spectral (XS) and panchromatic (PAN) images were used. A fusing technique (Liu 2000) was used to produce a higher resolution false-color composite image to facilitate landslide recognition. The pixel resolution after fusing was 10 m.

The DEMs were acquired from the Department of Interior, Taiwan and were visually checked using a color-shaded image of the DEM. When a defect of more than a few pixels in size was found, this portion was re-digitized from a 1:5,000 scale photo-based contour map. Other abnormal random points were corrected using a median filter. Finally the DEM was smoothed a little and reduced to a 10 m grid for subsequent analyses.

Geological maps (1:50,000) were obtained from the Central Geological Survey, Taiwan. Each map was overlaid with a shaded DEM and visually inspected in GIS. Some abnormal boundaries, mostly associated with alluvial and terrace deposits, were corrected. The Erdas Imagine system was used to transform the geologic vector map to a raster image of 10 m pixels.

Digital strong-motion seismograms were collected by the Central Weather Bureau, Taiwan. They were acquired and processed for ground-

Table 22.1 List of satellite images used in establishing the landslide inventory

Location	Event date	Image	Date	Type
Tahan	1999/09/21	Before	1999/02/18, 1999/04/01, 1999/08/17	XS & PAN
		After	2000/01/02, 2000/01/29	
Fongshan etc.		Before	1999/04/01	
		After	1999/09/27, 1999/10/31, 2000/01/29	
Taan		Before	1999/04/01, 1999/04/02	
		After	1999/10/04, 1999/10/31	
Dajia		Before	1998/07/16, 1999/04/01	
		After	1999/10/31, 2000/01/08	
Wu		Before	1999/04/01, 1999/04/08	
		After	1999/10/31	
Jhuoshuei		Before	1999/04/01, 1999/09/11	
		After	1999/10/31, 1999/11/17, 2000/01/08	
Other area		Before	1999/04/01, 1999/07/01, 1999/07/24	
		After	1999/09/26, 1999/09/27, 1999/10/12	

motion parameters (landslide triggering factors) in this study.

All the vector layers were converted into raster cells of 10 × 10 m in size and these were used for all subsequent processing and analysis for each landslide factor.

4.1 Landslide Mapping

False-color images were used for landslide recognition. Image interpretation was based on image tone, shape, association, and also personal experience. The landslides were digitized in GIS and attributes assigned to establish a landslide map table. Each landslide table was then checked against recent rectified aerial photographs via the GIS. Most misinterpretations due to man-made features or cultivated land could be recognized during this comparison. The landslide tables were further modified using ground data obtained from field checks, and a landslide inventory was formed. Landslide types were noted after examining the characteristics of the landslide's shape, scarring, and deposition on SPOT images, photo-based maps, and by field checking. These data were also recorded as attributes for each landslide object in the GIS.

Rock falls were further analyzed by using slope gradients. They were found largely to be located on slopes >55°, with almost none on slopes of <50°. Rock-fall zones were then defined to be the region where slopes are >50° and where the area is larger than 0.5 ha. Finally the attributes in the database were updated using these rock fall zones to refine the landslide types and differentiate between shallow slides and rock falls.

Landslide deposits were identified by comparing the GIS landslide layer with the 1:5,000 scale photo-based contour maps. The slope angle or concentration of contour lines was used to differentiate deposit from source areas. The final GIS landslide inventory included a detailed description of the date/event, source/deposit, size and type of each landslide object. Finally, a pre-event, a post-event, and an event-triggered landslide inventories were made.

4.2 Event-Based Landslide Inventory

An event-triggered landslide was identified by comparing the pre-event and post-event landslide inventories, and an event-based landslide

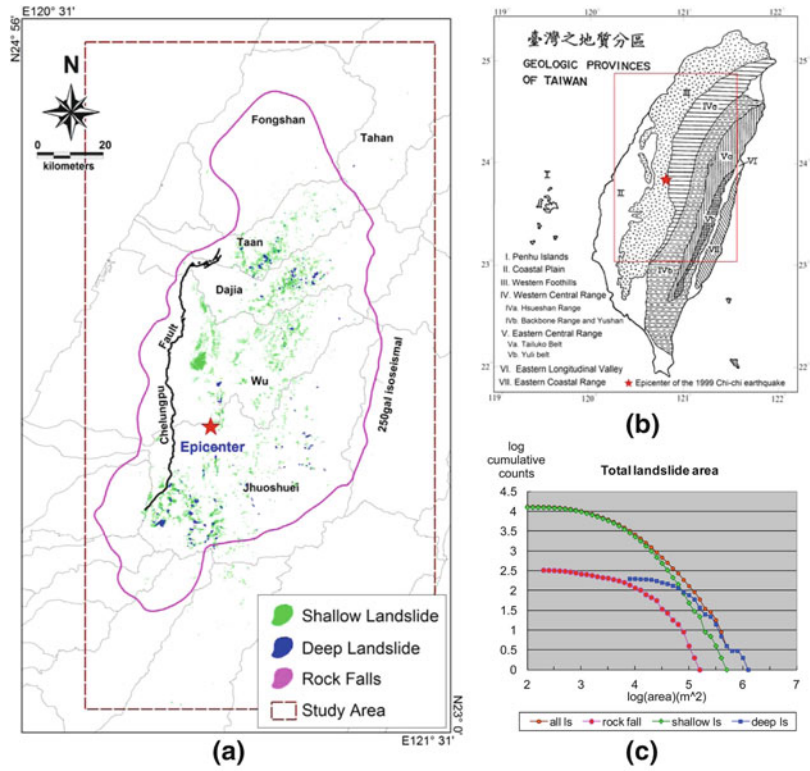

Fig. 22.1 Landslides triggered by the 1999 Chi–Chi earthquake: **a** Landslide distribution, *red* star indicates epicenter of the Chi–Chi earthquake. **b** Index map with geology of Taiwan. **c** Size distribution of landslides

Table 22.2 List of Chi–Chi earthquake-induced landslides

Type	Number	Area (km^2)	Number[a]	Area (km^2)[a]
Rock falls	326	4.493	310/16	4.291/ 0.202
Shallow slides	12,651	90.177	12,198/ 453	86.778/ 3.399
Deep slides	198	24.834	195/3	24.567/ 0.267
All	13,175	119.504	12,703/ 472	115.636/ 3.868

[a] *Note* Landslides within/outside 250 gal isoseismal

inventory was produced. An event-triggered landslide could be absent from the pre-event landslide inventory, or present in both inventories. Landslides found in both inventories were carefully examined for changes in tone and/or enlargement in extent. The Chi–Chi earthquake event-based landslide inventory is shown in Fig. 22.1, and the number and area of landslides is listed in Table 22.2.

Landslides triggered by the Chi–Chi earthquake include rock falls, shallow slides, and deep-seated landslides. Most landslides occurred within the 250-gal isoseismal line of earthquake shaking. The deep-seated landslides include two structurally controlled landslides: the Tsaoling landslide and the Chiufengerhshan landslide. Landslides due to lateral spreading were not found in this event.

4.3 Processing of Landslide Causative Factors

We selected several frequently used landslide factors for analysis: lithology, slope gradient, slope aspect, roughness, curvature, slope height, distance to a road, distance to the earthquake source, and earthquake intensity. The data set for each factor was first divided into a *landslide* group and a *non-landslide* group. Data for each group were then classed into intervals and the number of pixels in each interval recorded for plotting the frequency distribution of a group.

The distribution of these two groups was visually inspected and a standard difference between the two groups was calculated.

The landslide ratio for each interval of factor score was calculated first, then plotted to form a landslide probability curve. It was then ready for visual inspection and calculation of a correlation coefficient.

The cumulative landslide probability was then plotted to form a success-rate curve and the AUC was calculated. The superiority of a factor was mostly quantified by the area under the success rate curve.

4.4 Processing of Landslide Triggering Factors

Landslide triggering factors associated with earthquake shaking are related to intensity. These may include peak ground acceleration (PGA), peak ground velocity (PGV), and Arias Intensity (AI), all of which are obtained from the earthquake strong-motion records.

The strong-motion data required initial baseline correction and filtering. These were carried out using standard procedures suggested by the Pacific Earthquake Engineering Research Center (PEER) (Darragh et al. 2004). PGA, PGV and AI were then calculated from each corrected seismogram. The arithmetical mean of the Arias Intensities of the N–S and E–W components was used to represent the earthquake intensity for the strong-motion station site. The geometrical mean of the PGA of the N–S and E–W components were used to represent the horizontal PGA for the strong-motion station site. The geometrical mean of the PGV was also calculated in this way. These values were interpolated on each grid point in the study area using ordinary kriging. Stations located on the tops of ridges were not included in the interpolation.

5 Landslide Controlling Factors and Evaluation

Eight factors were evaluated as more effective for interpreting the landslide spatial distribution.

5.1 Lithology

Geological conditions as well as lithology have a great influence on landslides. The Pleistocene Toukoshan Formation, the Pliocene Series, the Upper Miocene Groups, and the Eocene quartzitic sandstone and slate are more easily influenced by earthquake shaking. The Huoyenshan Conglomerate in the Toukoshan Formation is especially sensitive to an earthquake.

5.2 Slope Gradient

Slope gradient is an important factor controlling landslide occurrence. The present study confirms previous results that more landslides occur on steeper slopes (Fig. 22.2). It reveals a threshold at a gradient of about 40 % and shows a very good positive correlation with the slope gradient. The area under the success rate curve suggests that it is a good factor for all types of landslides. The area under the curve is as high as 0.916 for rock falls, 0.765 for shallow slides, and 0.727 for deep-seated slides.

5.3 Slope Aspect

Earthquake shaking may have a preferred orientation, so landslides may occur more frequently on slopes with a certain aspect. The present study (Fig. 22.3) confirms previous results that more S- and SE-facing slopes collapsed during the Chi–Chi earthquake. This may be explained by the movement of the thrust block, which was moving to the NW and N direction and confirms the results of Ji et al. (2003).

5.4 Slope Curvature

Convex slope surfaces are more stable than concave slope surfaces. The present results generally show a positive correlation between landslide occurrence and curvature. However, Fig. 22.4 shows that among the four curvature measures,

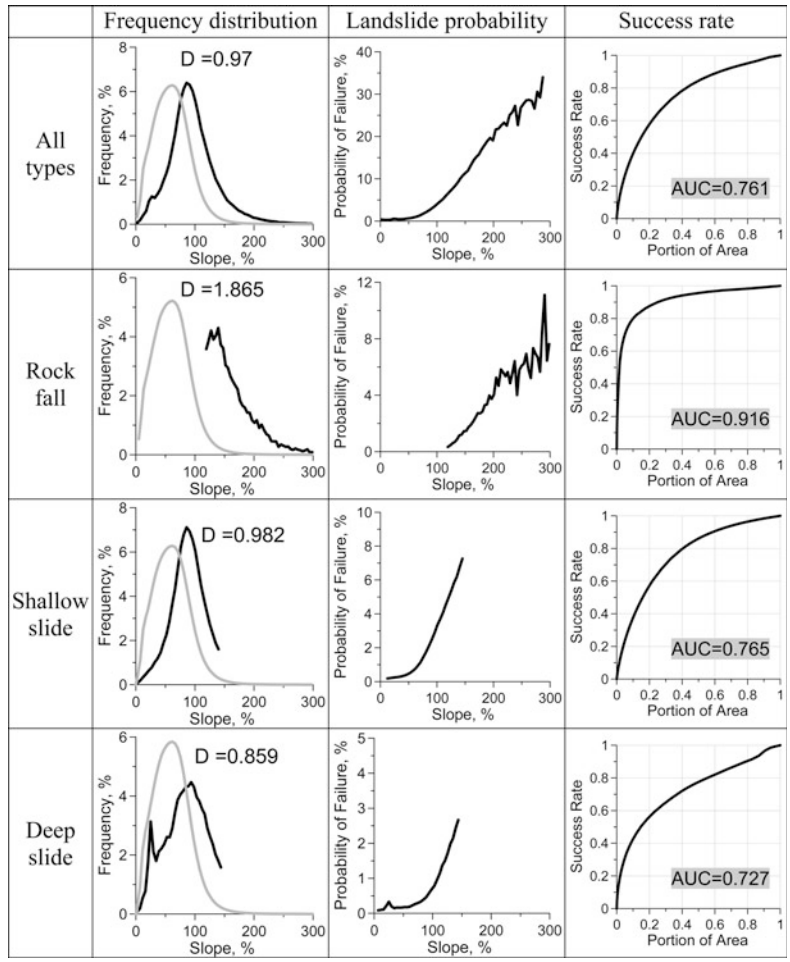

Fig. 22.2 Differences in slope-gradient factor between landslide and non-landslide groups, landslide probability, and success rate counted within 250 gal isoseismal

only total curvature showed a fairly good success rate (AUC = 0.634), others are very poor.

5.5 Slope Height

Storm-induced landslides are more common on lower slopes and show a negative correlation with slope height, whereas earthquake-induced landslides are located closer to ridge tops and show a positive correlation with slope height in general. The results of present study show that earthquake-induced landslides have only a poor correlation to the total-slope-height factor (AUC = 0.577), and have a very poor correlation to the local-slope-height factor and the relative-slope-height factor (Fig. 22.5). Relative-slope-height is defined as the ratio of local-slope-height to total-slope-height and ranges from 0 (toe of slope) to 1 (top of slope).

5.6 Distance to Earthquake Source

We have compared the correlation of landslide occurrence using four different definitions of distance: (1) distance to epicenter, (2) distance to hypocenter, (3) distance to fault-rupture line, and (4) distance to fault-rupture plane. The distance-to-fault-rupture-plane and distance-to-fault-rupture-line are both the factors most affecting landslide occurrence (AUC = 0.661 ~ 0.663), and distance-to-epicenter and distance-to-hypocenter are also both effective factors (AUC = 0.632 ~

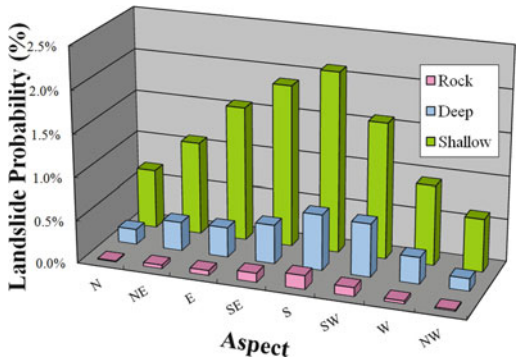

Fig. 22.3 Landslide probability for different slope aspects in three types of landslide, counted within 250 gal isoseismal

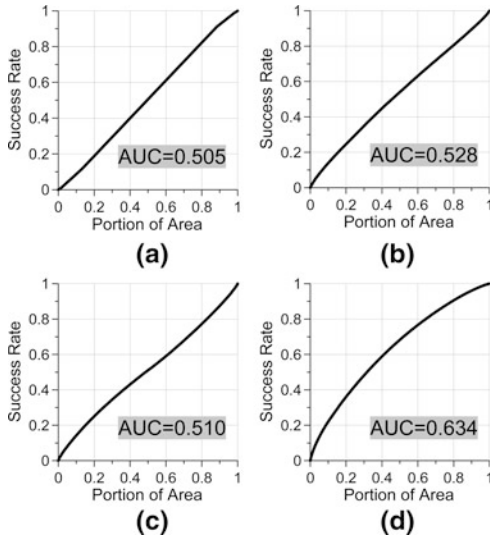

Fig. 22.4 Success rate curves for curvature factors to interpret shallow landslides within 250 gal isoseismal: **a** Plane curvature. **b** Profile curvature. **c** Tangential curvature, and (**d**) total curvature

0.633) (Fig. 22.6). Data on the fault rupture plane was calculated from Cheng et al. (2000).

5.7 Intensity of Ground Shaking

We compared landslide occurrence to three different definitions of intensity: (1) peak ground acceleration (PGA), (2) peak ground velocity (PGV), and (3) Arias Intensity. We found that the three intensity measures are all effective, but the Arias Intensity was the most effective factor for interpreting landslide occurrence. Arias Intensity was a good factor to explain all types of landslides (Fig. 22.7). The area under the success rate curve is as high as 0.714.

6 Characteristics of Earthquake-induced Landslides

Most landslides are either triggered by a storm rainfall or an earthquake. There are some differences in location and other characteristics between the former and the latter. Earthquake-induced landslides are located on steeper and longer slopes than the storm-induced ones, and preferably occur at a higher position on the slope and are closer to the ridge, whereas storm-induced landslides preferably occur at a lower slope position, closer to the river bank. This is clearly shown in Fig. 22.8, that most of the landslides triggered by the Typhoon Aere locate at lower relative slope height and are closer to the river bank (Fig. 22.8c), most landslides

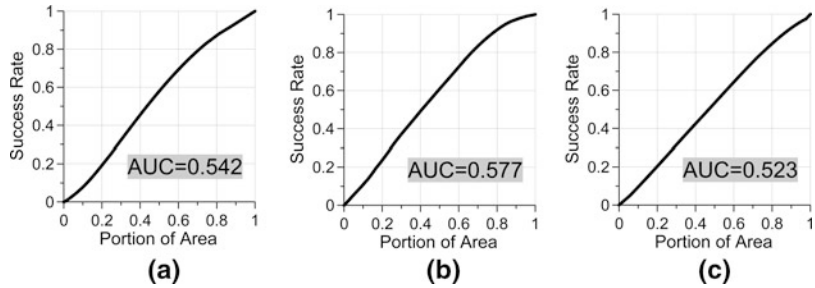

Fig. 22.5 Success rate curve for slope height factor for shallow landslides within 250 gal isoseismal: **a** Local slope height. **b** Total slope height, and (**c**) relative slope height

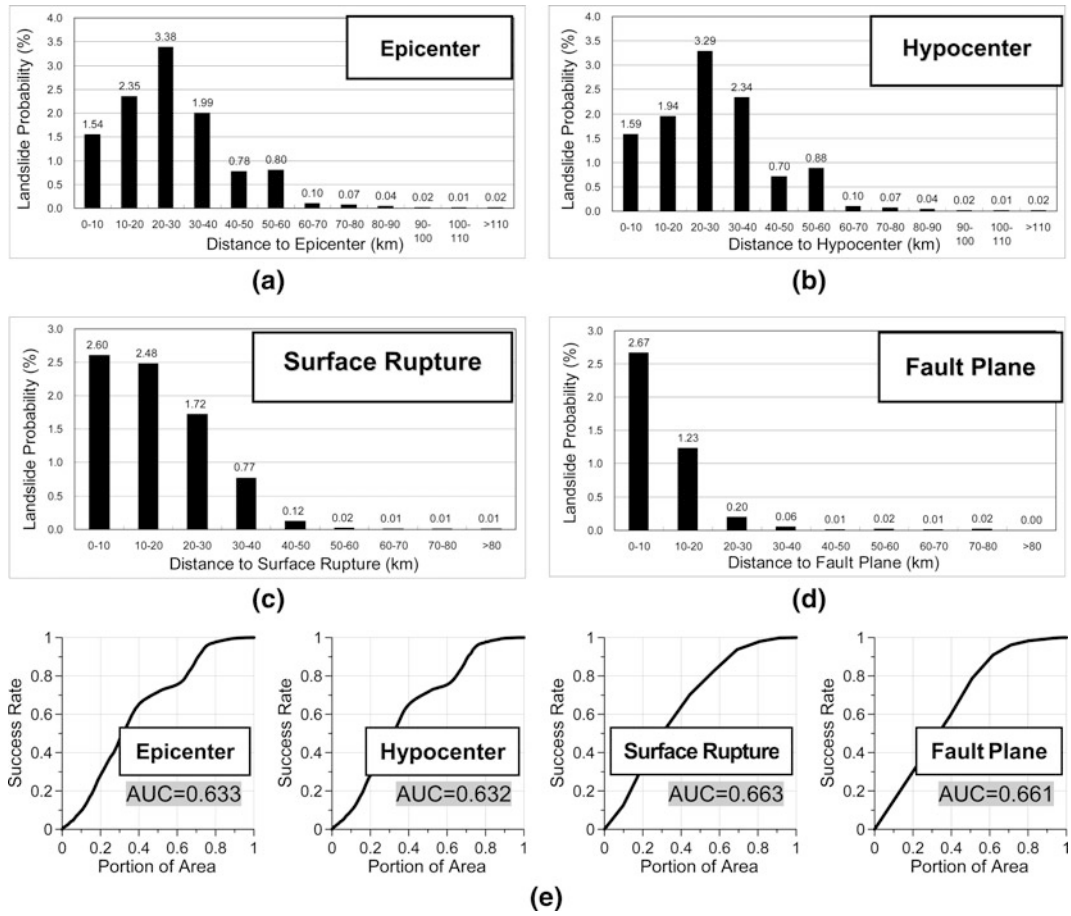

Fig. 22.6 Landslide probability (all types) for (**a**) epicenter distance. **b** Hypocenter distance. **c** Rupture-line distance, and (**d**) fault plane distance, and (**e**) success rate and area under the curve (AUC) computed within the 250-gal isoseismal

triggered by the Chi–Chi Earthquake locate at higher relative slope height closer to the ridge (Fig. 22.8a), whereas storm-induced landslides after the Chi–Chi Earthquake behave in between (Fig. 22.8b). Meunier et al. (2008) found similar results to our studies.

The storm-induced landslides may have a fairly good correlation with the relative-slope-height factor as shown in Fig. 22.8c. The earthquake-induced landslides are only poorly correlated with relative-slope-height factor, although their visual performance still is satisfactory (Fig. 22.8a). The total-slope-height factor is more effective than the relative-slope height factor, and indicates that it occur more landslides at a longer slope. The slope gradient factor is a good to excellent causative factor for earthquake-induced landslides. Summarizing these, earthquake-induced landslides are most common on longer and steeper slopes, and occurred at a high position on the slope. Topographic amplification may have played a very important role in the occurrence of the earthquake-induced landslides.

Since there are fewer steep and long slopes in the meizoseismal area in northeastern Japan as compared to mountain slopes in Taiwan, the relatively less occurrence of coseismic landslides during the 2011 magnitude 9.0 Tohoku Earthquake may be explained by this topographic

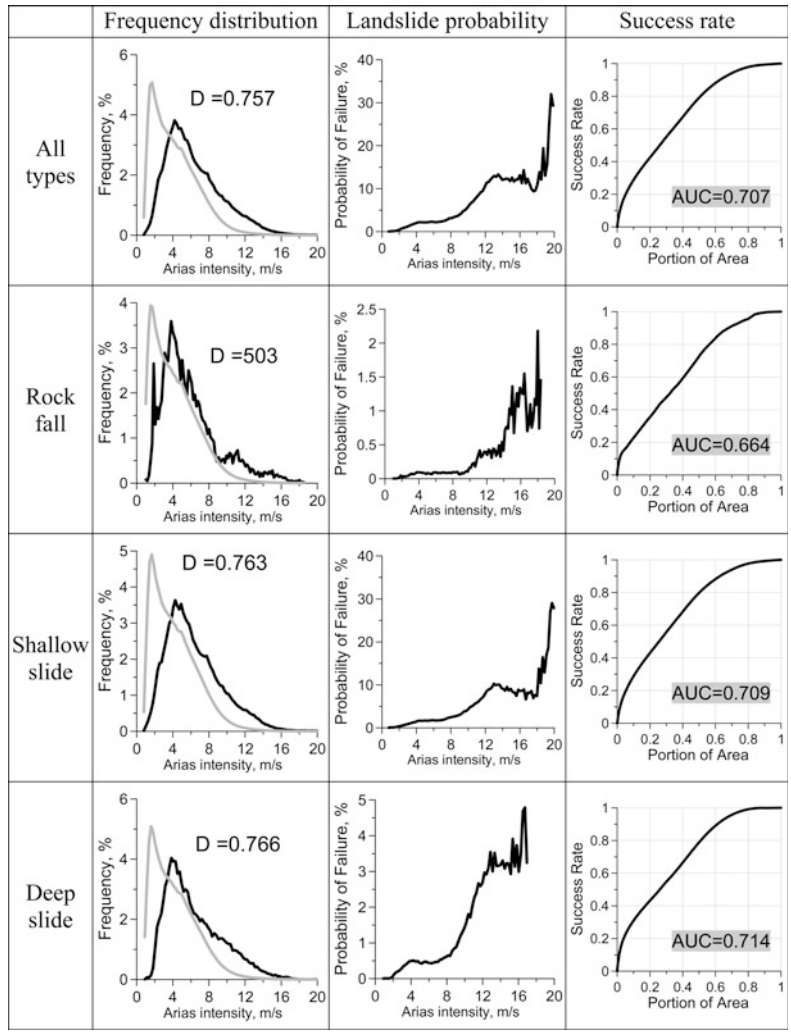

Fig. 22.7 Differences between landslide and non-landslide groups, probability of failure, and success rate counted within the 250-gal isoseismal for Arias Intensity factor

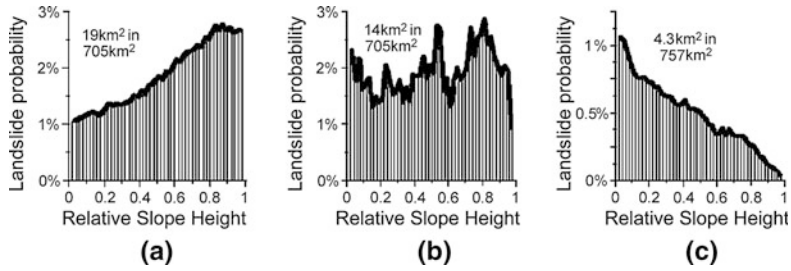

Fig. 22.8 Differences of landslide probability for: **a** Landslides triggered by the 1999 Chi–Chi Earthquake in Kuohsing quadrangle. **b** Landslides triggered by the 2001 Typhoon Toraji in Kuohsing quadrangle, and (**c**) landslides triggered by the 2004 Typhoon Aere in the catchment of Shihmen Reservoir

characteristics besides a possible interpretation by lithological characteristics which may be more resistant to earthquake shaking.

7 Conclusions and Recommendations

Landslides triggered by the 1999 Chi–Chi Earthquake were re-mapped from high-resolution SPOT images and checked by using aerial photo-pairs. Landslide types were recognized and deposit areas were separated, and all were associated with attributes in a GIS database. For earthquake-triggered landslides: (1) slope gradient was the most effective causative factor controlling the occurrence of landslides with an area under the success rate curve as high as 0.916 for rock falls, 0.765 for shallow slides, and 0.727 for deep-seated slides; (2) slope aspect showed some correlations to occurrence of landslides and reflected the fault movement direction; (3) total-slope-height factor roughly explained the occurrence of earthquake-induced landslides, but relative-slope-height could effectively explain the occurrence of storm-induced landslides which were commonly located closer to a river side; (4) closest distance to fault was the most significant source-distance factor associated with the landslides; and (5) Arias Intensity was the most significant intensity measure for interpreting landslide failures.

Most landslides were concentrated in the region exceeding 250 gals. Earthquake-induced landslides tended to occur on longer and steeper slopes and at a higher position on the slope, closer to the ridge. Topographic amplification may have played a very important role in the occurrence of the earthquake-induced landslides.

References

Bonilla MG (1975) A review of recently active fault in Taiwan. U.S. Geological survey open-file report 75–41, 58 p

Cheng CT, Lee CT, Tsai YB (2000) Fault rupture plane and attenuation model associated with the 1999 Chi–Chi earthquake. Proceedings of the 2000 annual meeting of the geological society of China, pp 21–23 in Chinese

Chung CF, Fabbri AG (1999) Probabilistic prediction models for landslide hazard mapping. Photogramm Eng Remote Sens 65:1389–1399

Dadson SJ, Hovious N, Chen H, Dade BW, Willett SD, Hu JC, Horng MJ, Chen MC, Stark CP, Lague D, Lin JC (2003) Links between erosion, runoff variability, and seismicity in the Taiwan orogen. Nature 426:648–651

Darragh B, Silva W, Gregor N (2004) Strong motion record processing for the PEER center. Proceedings of COSMOS invited workshop on strong-motion record processing, Richmond, California, USA, pp 26–27

Davis JC (2002) Statistics and data analysis in geology, 3rd ed. Wiley, Hoboken, 638 p

Ji C, Helmerger DV, Wald DJ, Ma KF (2003) Slip history and dynamic implications of the 1999 Chi–Chi, Taiwan, earthquake. J Geophys Res 108(B9):p. 2412

Jibson RW, Harp EL, Michael JA (2000) A method for producing digital probabilistic seismic landslide hazard maps. Eng Geol 58:271–289

Kao H, Chen WP (2000) The Chi–Chi earthquake sequence: active out-of-sequence thrust faulting in Taiwan. Science 288:2346–2349

Khazai B, Sitar N (2003) Evaluation of factors controlling earthquake-induced landslides caused by Chi–Chi earthquake and comparison with the Northridge and Loma Prieta events. Eng Geol 71:79–95

Lee CT, Huang CC, Lee JF, Pan KL, Lin ML, Dong JJ (2008a) Statistical approach to earthquake-induced landslide susceptibility. Eng Geol 100:43–58

Lee CT, Huang CC, Lee JF, Pan KL, Lin ML, Dong JJ (2008b) Statistical approach to storm event-induced landslide susceptibility. Nat Hazard Earth Syst Sci 8:941–960

Lee CT, Pan KL, Lin ML (2005) Research of landslide susceptibility analyses. Taiwan Central Geol Surv Open-File Rep 94–18, 474 p

Liao HW, Lee CT (2000) Landsides triggered by the Chi–Chi Earthquake. Proceedings of the 21st Asian conference on remote sensing. Volume 1&2:383–388

Liu JG (2000) Smoothing filter-based intensity modulation: a spectral preserve image fusion technique for improving spatial details. Int J Remote Sens 21(18):3461–3472

Ma KF, Lee CT, Tsai YB (1999) The Chi–Chi, Taiwan earthquake: large surface displacements on an inland fault. EOS Trans Am Geophys Union 80(50):605–611

Meunier P, Hovius N, Haines JA (2008) Topographic site effects and the location of earthquake induced landslides. Earth Planet Sci Lett 275:221–232

Teng LS (1990) Geotectonic evolution of late Cenozoic arc-continent collision in Taiwan. Tectonophysics 183:57–76

Tsai YB, Teng TL, Chiu JM, Liu HL (1977) Tectonic implications of the seismicity in the Taiwan region. Mem Geolog Soc China 2:13–41

Yu SB, Chen HY, Kou LC (1997) Velocity field of GPS stations in the Taiwan area. Tectonophysics 274:41–59

Wang WN, Nakamura H, Tsuchiya S (2002) Distributions of landslides triggered by the Chi-Chi Earthquake in central Taiwan on September 21, 1999. Landslides 38:18–26

Wu FT (1978) Recent tectonics of Taiwan. J Phys Earth 26(Suppl):265–299